This article is published as part of the *Dalton Transactions* themed issue entitled:

New Talent Asia

Highlighting the excellent work being carried out by younger members of the inorganic academic community in Asia

Guest Editor Masahiro Yamashita
Tohoku University, Japan

Published in issue 10, 2011 of *Dalton Transactions*

Image reproduced with permission of Kenneth Kam-Wing Lo

Articles in the issue include:

PERSPECTIVES:

ARTICLES:

Visit the *Dalton Transactions* website for more cutting-edge inorganic and organometallic research
www.rsc.org/dalton

Dalton Transactions

Dynamic Article Links

Cite this: *Dalton Trans.*, 2011, **40**, 2332

www.rsc.org/dalton

PAPER

Preparation and electrochemical properties of MnO_2 nanosheets attached to Au nanoparticles on carbon nanotubes

Li Wei, Changqing Li, Haibin Chu and Yan Li*

Received 20th August 2010, Accepted 10th November 2010
DOI: 10.1039/c0dt01073a

A wet chemical route for the preparation of MnO_2 nanosheet/Au nanoparticle/MWNT hybrid materials is developed. The Au nanoparticles are prepared by reducing $AuCl_4^-$ with citrate and attached to thiol-modified MWNTs. Owing to the reducing property and the binding ability to Mn-containing species of capping agents surrounded the Au nanoparticles, the MnO_2 nanosheets are formed on the surface of Au nanoparticles. The ternary nanocomposites of MnO_2/Au/MWNT have been characterized by transmission electron microscopy, X-ray diffraction, X-ray photoelectron spectroscopy, and FT-IR spectroscopy. The affiliation of MnO_2 nanosheets into the hybrids remarkably enhances the electrocatalytic performance of Au nanoparticle/MWNT towards the oxygen reduction reaction. The specific capacitance of the ternary hybrids is also increased dramatically comparing with that of Au/MWNT.

Introduction

Carbon nanotubes (CNTs) are hollow nano-sized tubes of concentric graphitic carbon capped by fullerene-like hemispheres.[1] CNTs have intrinsic properties, such as low density, high surface area, high stability, high electrical conductivity, and stability in acid/basic media. Owning to their excellent properties CNTs have been intensively studied in the last decade.[2–6] Inorganic nanomaterials are of particularly interest due to their unique electronic, optical, magnetic and catalytic properties. Importantly, these features differ from those of the bulk materials and can be further tuned by controlling their composition, size and morphology.[7] CNTs can be used as support materials for the dispersion and stabilization of inorganic nanomaterials.[8–13] Such hybrids of CNTs and inorganic materials may integrate the unique properties of both components[8] and have found various applications in catalysis,[2,9,10] energy conversion,[11–16] sensor,[17,18] and analysis.[19] Using CNTs instead of carbon black to support the nanosized inorganic catalysts in electrocatalytic processes is advantageous owing to the higher conductivity and stability of CNTs.[12]

Nowadays, the substitution of Pt in fuel cell and other electrochemical devices is attracting great attention. Au is believed to be one of the most promising candidate materials for non-Pt-based electrocatalysts in oxygen reduction reaction (ORR).[20] Yet, in acidic media a 2-electron reduction of oxygen takes place on the Au surface, while the peroxide intermediate is further reduced only at high over-potentials. Although the electron transfer number increases along with the decrease of the size of Au particles, the contribution of the two-electron reduction pathway of O_2 to hydrogen peroxide is still unavoidable at low potential even when the Au nanoparticles are smaller than 3 nm.[21] Manganese oxides have an excellent catalytic activity towards the chemical disproportionation of hydrogen peroxide into water and molecular oxygen. Therefore, a combined use of manganese oxide nanostructures together with Au nanoparticles might provide efficient electrocatalysts towards ORR. EI-deab *et al.* studied the activity of binary catalysts of Au nanoparticles and manganese oxide (MnO_x) nanoparticles electrodeposited onto glassy carbon electrode (GCE) towards ORR in alkaline medium.[22,23] They showed that the combined use of MnO_x and Au nanoparticles resulted in the occurrence of the ORR at a potential close to that obtained at Pt electrodes. However, the addition of MnO_x decreases the conductivity of the catalysts, which is unfavourable for the electrocatalysis.

Our strategy for this study is combining CNTs, Au nanoparticles, and nanostructured MnO_2 in a controlled way to obtain superior functions of the materials. Here, MnO_2 nanosheets were attached to Au nanoparticles supported on carbon nanotubes through a wet chemical route. The formation mechanism of the nanostructured composites was discussed. The electrocatalytic properties of the as-obtained hybrid materials towards ORR was studied on bare GCE using cyclic voltammetry (CV) and liner scanning voltammetry (LSV). The results show that the integration of CNTs and Au with MnO_2 is promising to obtain improved electrocatalytic performance.

In addition, MnO_2 is considered to be an important candidate material for supercapacitors. The electrochemical performance of MnO_2 depends on their crystallographic forms, specific surface area, morphology and electrical conductivity.[24,25] However, the low

Beijing National Laboratory for Molecular Sciences, State Key Laboratory of Rare Earth Materials Chemistry and Applications, Key Laboratory for the Physics and Chemistry of Nanodevices, College of Chemistry and Molecular Engineering, Peking University, Beijing, 100871, China

electrical conductivity of MnO_2 is unfavourable for fast electron transfer during the electrochemical processes. The combination of MnO_2 with CNTs may compensate the poor conductivity.[26] Therefore, we also investigated the capacitance properties of the hybrids.

Experimental

Thiolation of MWNTs

Purified MWNTs with diameters of 10–20 nm were purchased from Shenzhen Nanotech Port Co. Ltd, China. The as-received MWNTs were oxidized by refluxing at 130 °C in concentrated nitric acid for 12 h, followed by washing with deionized water for several times and dried at 70 °C for 10 h. The surface thiolation of MWNTs were performed by the dicyclohexycarbodiimide (DCC)-assisted condensation reaction between carboxyl groups on the surface of oxidized MWNTs and amino groups of $NH_2(CH_2)_2SH$. Typically, 0.1 g oxidized MWNTs were first dispersed in 100 ml N,N-dimethylformamide (DMF) by sonication, then 0.6 g DCC and 0.2 g $NH_2(CH_2)_2SH$ were ultrasonically dissolved in the suspension. The condensation reaction was carried out by stirring the reaction solution at 50 °C for 6 h. After that, the thiol-modified MWNTs (s-MWNTs) were collected by centrifugation and washed with ethanol, then dried in vacuum at room temperature for 6 h.

Preparation of Au nanoparticle/MWNT hybrid materials

The Au colloid was prepared *via* reduction of $HAuCl_4$ with sodium citrate as reported by Turkevich.[27] For a typical procedure, 25 mL 0.01 wt% $HAuCl_4$ solution was stirred and heated to boiling, then 1 mL 1 wt% sodium citrate solution was added quickly. After being boiled for 10 min, the solution was cooled to room temperature. Subsequently, the Au colloid was mixed with 5 mg s-MWNTs dispersed in 25 mL deionized water under sonication.

Synthesis of MnO_2 nanosheets on the surface of Au nanoparticles attached to MWNTs

10 mL 0.01 M $KMnO_4$ solution was added to the Au/MWNT composite suspension. The mixture was kept at 70 °C for 2 h under mechanical stirring. Then the suspension was centrifuged at 12 000 rpm for 20 min, washed with deionized water and ethanol and dried in vacuum at room temperature.

Characterization

Transmission electron microscopy (TEM, JEOL-200 CX) and high-resolution TEM (HRTEM, Tecnai F30) were employed to examine the morphology and the size of the hybrid materials. X-ray diffraction (XRD) measurements were performed on a Rigaku Dmax-2000 X-ray diffractometer using Cu-Kα radiation (λ = 1.5406 Å) with an accelerating voltage of 40 kV. The IR spectra of the samples were measured on a Magna-IR 750 Fourier transform infrared (FTIR) spectrometer at a resolution of 4 cm^{-1}. X-ray photoelectron spectroscopy (XPS) measurements were performed on a AXIS Ultra X-ray photoelectron spectroscope with Al-Kα radiation ($h\nu$ = 1486.71 eV).

Electrochemical measurements

Electrochemical measurements were performed on an electrochemical workstation (CHI660C) by cyclic and linear scanning voltammetry technique. Ag/AgCl/KCl(saturated) electrode and Pt wire were used as reference and counter electrodes, respectively. For the liner scanning voltammetry measurements, rotating disk electrode (Pine Research Instrument) with glassy carbon (GC) substrate was used as working electrode. The catalyst-modified electrode was prepared by transferring 10 μL suspension of the samples onto the glassy carbon electrode with a diameter of 3.0 mm (5.0 mm for RDE). After the electrode was dried, the hybrid material was covered with a thin layer of Nafion to ensure the adherence to the electrode surface. ORR was carried out in O_2-saturated 0.1 M KOH aqueous solutions at room temperature. The capacitance performance of the samples was investigated with similar procedure in 0.5 M Na_2SO_4 aqueous solution while a saturated calomel electrode (SCE) was used as the reference electrode instead.

Results and discussion

1. Self-assembly of Au nanoparticles on MWNTs

TEM image of Au particles anchored on MWNTs by sonication method was shown in Fig. 1a. In the citrate-reduction procedure, the Au nanoparticles were produced by the reduction of $AuCl_4^-$ and stabilized by dicarboxy acetone molecules.[27] When Au sol was mixed with s-MWNTs suspension, Au nanoparticles linked to the CNTs by the strong coordination interaction between Au and S. Under the sonication condition, the presence of transverse shear force can help to obtain a suspension with good dispersion and thus increase the combination chance of Au nanoparticles with the outside walls of s-MWNTs.

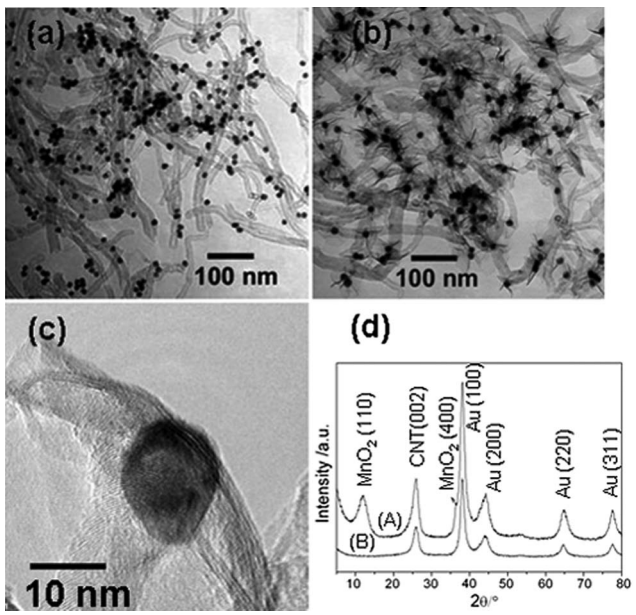

Fig. 1 (a) TEM image of Au particles anchored on MWNTs with sonication method; (b, c) TEM and HRTEM images of MnO_2/Au/MWNT hybrid materials; (d) XRD patterns for MnO_2/Au/MWNT (A) and Au/MWNT (B).

2. Structure of MnO_2 nanosheet/Au nanoparticle/MWNT hybrids

Fig. 1b and 1c show the TEM and HRTEM images of the MnO_2/Au/MWNT hybrid materials prepared *via* heating Au nanoparticle/MWNT in $KMnO_4$ solution at 70 °C for 2 h. It can be seen from Fig. 1b that nanosheets with less than 100 nm in length were attached onto the surface of Au nanoparticles anchored on MWNTs. The HRTEM characterization showed that the nanosheets were about ~10 nm in width and 100 nm in length. Additionally, the lattice fringes with interplanar distances of approximately 0.23 nm correspond to the {211} planes of α-MnO_2.

Fig. 1d shows XRD patterns for Au/MWNT and MnO_2/Au/MWNT hybrids. Both samples show characteristic peak of MWNTs at $2\theta = 25.78$ (002), the other peaks in Fig. 1d(B) can be indexed to a cubic phase Au (JCPDS no. 04-0784). Fig. 1d(A) shows a broad diffraction peak at $2\theta = 12.0$ and a shoulder peak at $2\theta = 36.7$, which correspond to {110} and {400} planes of α-MnO_2 (JCPDS 44-0141), respectively.

3. Effect of reaction time on the morphology of the hybrid materials

The reaction time not only determines the size and the density of MnO_2 nanosheets, but also affects the aggregation and size variation of Au nanoparticles. As the reaction time was prolonged from 2 to 8 h, the density of MnO_2 nanosheets was remarkably increased (Fig. 2). Meanwhile, the average length of the nanosheets increased from 35 to 50 nm. Once the reaction time was extended to 16 h, the size of Au nanoparticles increased, accompanied by the length shortening of MnO_2 nanosheets. The size increase of Au nanoparticles probably results from the lack of protection due to the oxidation of the stabilizer molecules on the surface of Au nanoparticles after heating in $KMnO_4$ solution at 70 °C.

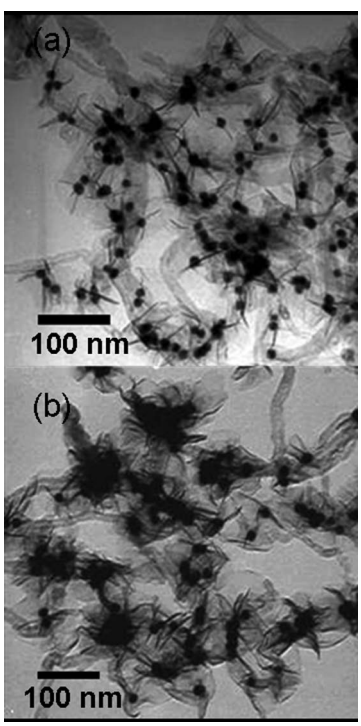

Fig. 2 TEM images of MnO_2/Au/MWNT hybrid materials prepared by heating Au/MWNT in 1.67 mM $KMnO_4$ solution at 70 °C for 8 h (a) and 16 h (b).

4. Formation mechanism of MnO_2 nanosheets

Typical XPS spectra of MnO_2/Au/MWNT hybrid materials is shown in Fig. 3a. The oxidation state of manganese can be evaluated from Mn 2p spectrum. From Fig. 3a we can see that Mn $2p_{3/2}$ and Mn $2p_{1/2}$ peaks are centered at 642.6 eV and 654.4 eV, respectively, with a spin-energy separation of 11.8 eV, which is in accordance with the reported data of Mn $2p_{3/2}$ and Mn $2p_{1/2}$ in MnO_2.[24,28] In addition, no Mn $2p_{3/2}$ signal of Mn_2O_3 (641.2 ± 0.2 eV) and $KMnO_4$ (647 eV) were observed in the XPS spectra, indicating that the oxidation state of Mn is +4.

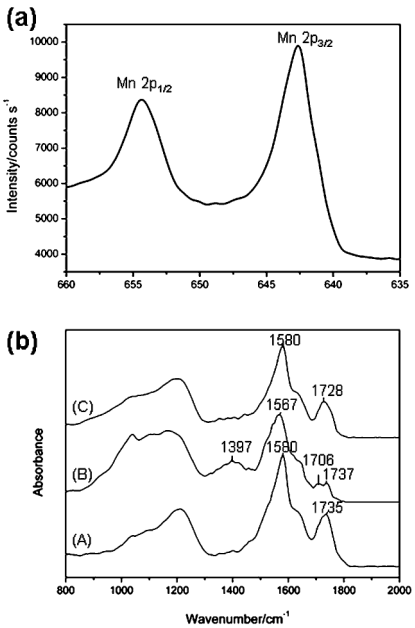

Fig. 3 (a) XPS spectrum of Mn 2p for MnO_2/Au/MWNT hybrid material; (b) FTIR spectra of s-MWNTs (A), Au/MWNT (B) and MnO_2/Au/MWNT (C).

The change of surface group of Au NPs can be verified from FTIR spectra (Fig. 3b). For s-MWNTs, the bands located at 1735 cm^{-1} and 1580 cm^{-1} are ascribed to the $\upsilon_{(C=O)}$ mode of amide groups and the stretching mode of C=C in CNTs, respectively. For Au/MWNT, the band around 1706 cm^{-1} is attributed to the $\upsilon_{(C=O)}$ of stabilizer molecules on Au surface. Meanwhile, the peak at 1397 cm^{-1} and 1567 cm^{-1} are assigned to the symmetric and asymmetric stretching bands of carboxylate group in the stabilizer molecules, respectively.[29] However, these characteristic IR adsorption bands of stabilizer molecules on Au surface disappear in the spectrum of the MnO_2/Au/MWNT composite, as shown in Fig. 3b(C). This is the evidence that the stabilizer molecules were oxidized by $KMnO_4$ when heating at 70 °C, meanwhile, MnO_2 nanosheets were formed *in situ* on the surfaces of Au nanoparticles by the reduction of $KMnO_4$.

In order to further investigate the formation mechanism of the MnO_2/Au/MWNT ternary hybrids, MnO_2/Au and MnO_2/MWNT hybrids were prepared, respectively. As shown in Fig. 4, MnO_2 nanosheets only formed on the surface of Au

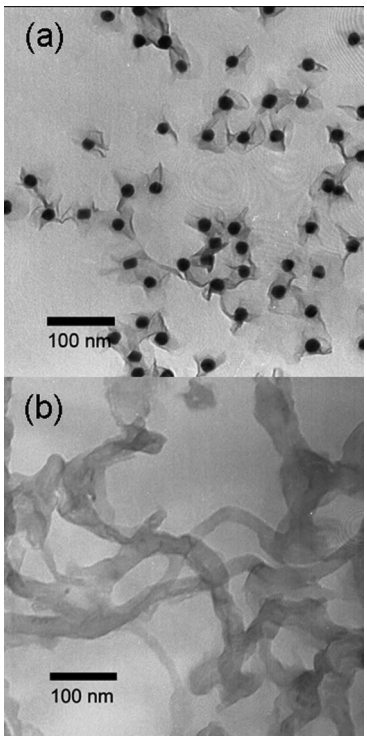

Fig. 4 TEM images of Au/MnO_2 (a) and MnO_2/MWNT (b).

nanoparticles, while no MnO_2 nanosheets are observed on the surface of MWNTs without Au nanoparticles, but the MWNTs are different from their raw morphology and there are some attachments adhered on the surface of MWNTs. Previous studies have revealed that on the surface of MWNTs, MnO_4^- can be reduced to MnO_2 by oxidizing exterior carbon, forming MnO_2 coated MWNTs.[13,30] So the attachments on MWNTs may be amorphous MnO_2 formed by the reduction of MnO_4^-.

On the basis of our experimental result, it is reasonable to assume that Au nanoparticles play a critical role in the formation of MnO_2 nanosheets. A small quantity of H^+ formed during the formation of Au nanoparticles can promote the formation of acetone diacetate,[31] which located at the outside of protective agent. The Mn atoms of the MnO_6 octahedron, the basic unit of MnO_2, may form bonds with O atoms of the protective agents on the surface of Au nanoparticles *via* an intermolecular hydrogen bond or coordination bond, acting as anchor sites for the growing of MnO_2 nanosheets. Meanwhile, the capping agents of Au nanoparticles, *i.e.* citrate ions, could act as the reductants for MnO_4^-. Then the formation of MnO_2 nanosheets is initiated at the Au nanoparticles. When the concentration of $KMnO_4$ is moderate, MnO_2 nanosheets can only be formed around the Au nanoparticles. But if the initiate concentration is too high, the site selectivity of the growth of nanostructured MnO_2 goes off.

5. Electrochemical performances of the MnO_2/Au/MWNT hybrid materials

The electrochemical behaviour of MnO_2/Au/MWNT ternary hybrids towards ORR was studied in O_2-saturated 0.1 M KOH solution at a scan rate of 50 mV s^{-1}. ORR behaviour of bare GC electrode, Au/MWNT and MnO_2/Au/MWNT are shown in Fig. 5a. Compared with the cyclic voltammograms recorded in N_2-saturated 0.1 M KOH solution (Fig. 5b solid curve) and air-saturated 0.1 M KOH solution (Fig. 5b dotted curve), we can find that the oxygen reduction peak appears at ~ –0.39 V for bare GC electrode, while it appears at more positive potential for both Au/MWNT (Fig. 5c) and MnO_2/Au/MWNT hybrids (Fig. 5d). Further more, the reduction current of ORR increases evidently, indicating that Au/MWNT and MnO_2/Au/MWNT hybrids present good catalytic activity towards ORR. Fig. 5e shows the linear scanning voltammograms of ORR recorded on RDEs. The result shows that the ORR onset potential on MnO_2/Au/MWNT hybrids is about 0.0 V, whereas it is about –0.2V on Au/MWNT. In addition, MnO_2/Au/MWNT hybrids display higher limiting current density compared with that of Au/MWNT. The increase of peak current is attributed to the catalytic disproportional activity of MnO_2. This result is consistent with the results of previous studies, which revealed that Au nanoparticles were found to cause a significant positive shift of the onset potential of the current flow of the ORR, while MnO_x enhanced the catalytic disproportionation of the electrogenerated hydrogen peroxide.[22]

A peak at the potential of about –0.45 V is observed for MnO_2/Au/MWNT hybrids in Fig. 5a(C). And the peak did not disappear when the cyclic voltammogram was carried out in N_2-saturated 0.1 M KOH. So the peak may arise from the reduction of MnO_x. Further research is needed to fully address the reduction pathway of the ORR.

Cyclic voltammograms of Au/MWNT and MnO_2/Au/MWNT hybrids were also recorded between –0.2 and 1.0 V *vs.* SCE in aqueous 0.5 M Na_2SO_4 at a scan rate of 5 mV s^{-1}. MnO_2/Au/MWNT hybrids show better capacitance performance than Au/MWNT as shown in Fig. 5f. The specific capacitance (SC) of the electroactive material was calculated using the following equation,[32]

$$C = \frac{q}{\Delta V \times w}$$

where q is the voltammetric charge, ΔV is the potential window of cycling, and w is the loading of the composites. The SC values for all electrodes are listed in Table 1. It is inferred from Table 1 that the specific capacitance of MnO_2/Au/MWNT is 2–3 times higher than that of Au/MWNT, meantime the specific capacitance of MnO_2/Au/MWNT increases with the increase of reaction time, indicating that the MnO_2 nanosheets formed on the surface of Au nanoparticles show good capacity for charge storage. The nanosheets have a very small thickness of ~10 nm, hence the specific surface area should be very high. And the nanosheets are well crystallized. Therefore, theoretically, this kind of MnO_2 nanosheets ought to present superior capacitance. In respect that w is the loading of the composites and only a small amount of MnO_2 present in the composites, if the loading of MnO_2 was used instead, the specific capacitance would be much higher.

Table 1 Specific capacitance (SC) of Au/MWNT and MnO_2/Au/MWNT

Electrode materials	Specific capacitance /F g^{-1}
Au/MWNT	33.67
MnO_2/Au/MWNT (2 h)	99.6
MnO_2/Au/MWNT (8 h)	122.1

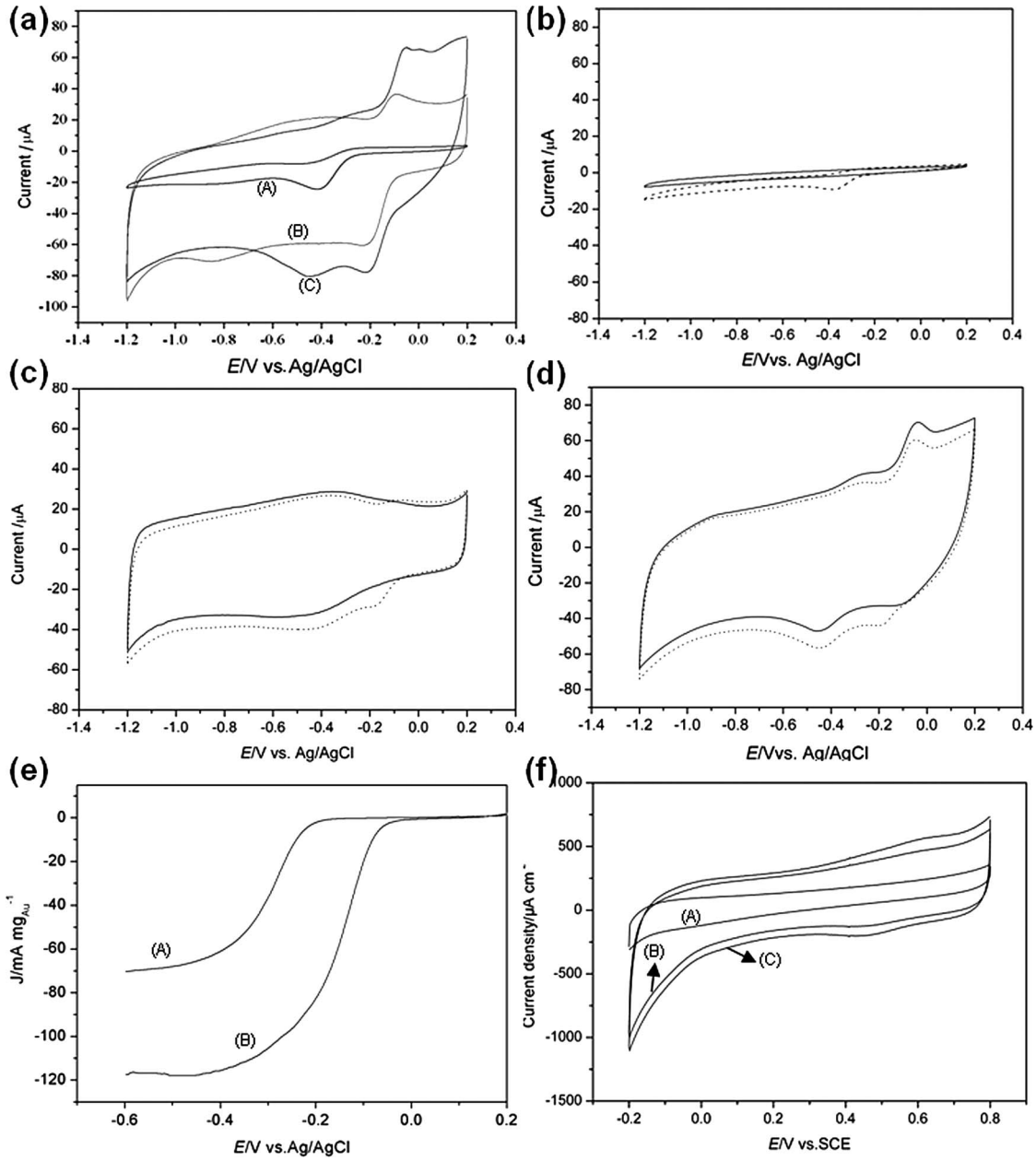

Fig. 5 (a) CVs for oxygen reduction at bare GC electrode (A), Au/MWNT (B) and MnO_2/Au/MWNT (C) in the O_2-saturated 0.1 M KOH solution; (b, c, d) CVs for oxygen reduction at bare GC electrode, Au/MWNT and MnO_2/Au/MWNT in the N_2-protected (solid curve) or air-saturated 0.1 M KOH solution (dotted curve); (e) Linear scanning voltammograms obtained at RDE coated with Au/MWNT (A), MnO_2/Au/MWNT (B) in O_2-saturated 0.1 M KOH solution at potential scan rate of 1 mV s^{-1}; (f) CVs of Au/MWNT (A) and Au/MnO_2/MWNT of different reaction time (B, 2 h; C, 8 h) in 0.5 M Na_2SO_4 aqueous solution.

Conclusion

Ternary hybrid materials composed of MnO_2 nanosheets, Au nanoparticles and MWNTs were prepared through a wet chemical route. The formation mechanism was carefully studied employing the controlled experiments and by the surface analysis and spectroscopic data of the products. It was proposed that the reduction of MnO_4^- and the formation of MnO_2 nanosheets were initiated at the surfaces of Au nanoparticles. The capping agents on the surfaces of Au nanoparticles play important roles for the *in situ* formation of MnO_2 nanosheets around Au nanoparticles. The size and density of the nanosheets could be tuned by increasing the reaction time. Combining the high conductivity of MWNTs, the catalytic activity of Au nanoparticles and MnO_2 nanosheets, the MnO_2/Au/MWNT hybrids show superior electrochemical performance. Attribute to the assistance of MnO_2, the ternary composites show enhanced electrocatalytic activity toward ORR reaction and might be a potential substitute for Pt-based electrocatalysts. In addition, the specific capacitance of MnO_2/Au/MWNT is 2–3 times higher than that of Au/MWNT. These results show that the introducing of nanostructured MnO_2 into the Au/MWNT system

remarkably improves the electrochemical property. The ternary nanostructured hybrids of MnO_2/Au/MWNT may find potential applications as electrocatalysts for fuel cells and as materials for super capacitors.

Acknowledgements

The authors would like to acknowledge funding from the Ministry of Science and Technology of China (projects 2011CB933003 and 2007CB936202) and the National Natural Science Foundation of China (project 50772002)

References

1 S. Iijima, *Nature*, 1991, **354**, 56–58.
2 J. M. Planeix, N. Coustel, B. Coq, V. Brotons, P. S. Kumbhar, R. Dutartre, P. Geneste, P. Bernier and P. M. Ajayan, *J. Am. Chem. Soc.*, 1994, **116**, 7935–7936.
3 B. M. Quinn and S. G. Lemay, *Adv. Mater.*, 2006, **18**, 855–859.
4 W. W. Zhou, Z. Y. Han, J. Y. Wang, Y. Zhang, Z. Jin, X. Sun, Y. W. Zhang, C. H. Yan and Y. Li, *Nano Lett.*, 2006, **6**, 2987–2990.
5 H. B. Chu, Z. Jin, Y. Zhang, W. W. Zhou, L. Ding and Y. Li, *J. Phys. Chem. C*, 2008, **112**, 13437–13441.
6 H. B. Chu, J. Y. Wang, L. Ding, D. N. Yuan, Y. Zhang, J. Liu and Y. Li, *J. Am. Chem. Soc.*, 2009, **131**, 14310–10316.
7 C. N. R. Rao, Müller Achim and C. A. K., *The Chemistry of Nanomaterials: Synthesis, Properties and Applications*, John Wiley, 2004.
8 H. B. Chu, L. Wei, R. L. Cui, J. Y. Wang and Y. Li, *Coord. Chem. Rev.*, 2010, **254**, 1117–1134.
9 X. L. Pan, Z. L. Fan, W. Chen, Y. J. Ding, H. Y. Luo and X. H. Bao, *Nat. Mater.*, 2007, **6**, 507–511.
10 J. C. Kang, S. L. Zhang, Q. H. Zhang and Y. Wang, *Angew. Chem., Int. Ed.*, 2009, **48**, 2565–2568.
11 Y. C. Xing, *J. Phys. Chem. B*, 2004, **108**, 19255–19259.
12 Z. Y. Lin, H. B. Chu, Y. H. Shen, L. Wei, H. C. Liu and Y. Li, *Chem. Commun.*, 2009, 7167–7169.
13 S. W. Lee, J. Kim, S. Chen, P. T. Hammond and S. H. Yang, *ACS Nano*, 2010, **4**, 3889.
14 Y. H. Lin, X. L. Cui, C. Yen and C. M. Wai, *J. Phys. Chem. B*, 2005, **109**, 14410–14415.
15 S. B. Ma, K. W. Nam, W. S. Yoon, X. Q. Yang, K. Y. Ahn, K. H. Oh and K. B. Kim, *J. Power Sources*, 2008, **178**, 483–489.
16 C. Q. Li, N. J. Sun, J. F. Ni, J. Y. Wang, H. B. Chu, H. H. Zhou, M. X. Li and Y. Li, *J. Solid State Chem.*, 2008, **181**, 2620–2625.
17 J. Kong, M. G. Chapline and H. J. Dai, *Adv. Mater.*, 2001, **13**, 1384–1386.
18 A. Star, V. Joshi, S. Skarupo, D. Thomas and J. C. P. Gabriel, *J. Phys. Chem. B*, 2006, **110**, 21014–21020.
19 S. Hrapovic, Y. L. Liu, K. B. Male and J. H. T. Luong, *Anal. Chem.*, 2004, **76**, 1083–1088.
20 Y. Lee, A. Loew and S. H. Sun, *Chem. Mater.*, 2010, **22**, 755–761.
21 T. Inasaki and S. Kobayashi, *Electrochim. Acta*, 2009, **54**, 4893–4897.
22 M. S. El-Deab and T. Ohsaka, *J. Electrochem. Soc.*, 2006, **153**, A1365–A1371.
23 M. S. El-Deab and T. Ohsaka, *Electrochim. Acta*, 2007, **52**, 2166–2174.
24 X. P. Dong, W. H. Shen, J. L. Gu, L. M. Xiong, Y. F. Zhu, Z. Li and J. L. Shi, *J. Phys. Chem. B*, 2006, **110**, 6015–6019.
25 S. Devaraj and N. Munichandraiah, *J. Phys. Chem. C*, 2008, **112**, 4406–4417.
26 Y. Hou, Y. W. Cheng, T. Hobson and J. Liu, *Nano Lett.*, 2010, **10**, 2727–2733.
27 J. Turkevich, P. C. Stevenson and J. Hillier, *Discuss. Faraday Soc.*, 1951, **11**, 55–75.
28 D. A. Pena, B. S. Uphade and P. G. Smirniotis, *J. Catal.*, 2004, **221**, 421–431.
29 S. Y. Lin, Y. T. Tsai, C. C. Chen, C. M. Lin and C. H. Chen, *J. Phys. Chem. B*, 2004, **108**, 2134–2139.
30 X. Jin, W. Zhou, S. Zhang and G. Z. Chen, *Small*, 2007, **3**, 1513–1517.
31 S. Kumar, K. S. Gandhi and R. Kumar, *Ind. Eng. Chem. Res.*, 2007, **46**, 3128–3136.
32 A. Zolfaghari, F. Ataherian, M. Ghaemi and A. Gholami, *Electrochim. Acta*, 2007, **52**, 2806–2814.